



# Glass-forming ability correlated with the liquid-liquid transition in Pd<sub>42.5</sub>Ni<sub>42.5</sub>P<sub>15</sub> alloy

En-Yi Chen<sup>a,b</sup>, Si-Xu Peng<sup>b</sup>, Liang Peng<sup>a,b</sup>, Marco Di Michiel<sup>c</sup>, Gavin B.M. Vaughan<sup>c</sup>, Yao Yu<sup>a,b,\*</sup>, Hai-Bin Yu<sup>b</sup>, Beatrice Ruta<sup>c,d</sup>, Shuai Wei<sup>e</sup>, Lin Liu<sup>a,\*</sup>

<sup>a</sup> State Key Laboratory of Materials Processing and Die & Mould Technology, School of Materials Science and Engineering, Huazhong University of Science and Technology, Wuhan 430074, China

<sup>b</sup> Wuhan National High Magnetic Field Center, Huazhong University of Science and Technology, Wuhan 430074, China

<sup>c</sup> ESRF—The European Synchrotron, CS40220, Grenoble 38043, France

<sup>d</sup> Univ Lyon, Université Claude Bernard Lyon 1, CNRS, Institut Lumière Matière, Villeurbanne, France

<sup>e</sup> I. Institute of Physics (IA), RWTH Aachen University, Aachen 52074, Germany

## ARTICLE INFO

### Article history:

Received 12 September 2020

Revised 23 October 2020

Accepted 23 October 2020

### Keywords:

Crystallization

Phase transformation kinetics

Metallic glass

Time-temperature-transformation

Nuclear magnetic resonance

## ABSTRACT

Alloy melts can solidify into metallic glasses if cooled fast enough to avoid crystallization. Glass-forming ability (GFA), a measure of the ease of vitrification, is vital for the fundamental understanding of glass formation, and is also crucial for the application of metallic glasses. Previous studies of GFA mainly focused on the undercooled liquid phase, while the influence of the evolution of the stable melts on GFA is rarely addressed. Here we show that the Pd<sub>42.5</sub>Ni<sub>42.5</sub>P<sub>15</sub> glass-forming liquid, in which a first-order liquid-liquid transition (LLT) takes place at  $T_{LL} = 1063$  K high above its liquidus temperature, shows significantly different GFA when quenched from the temperature above or below  $T_{LL}$ . Moreover, the pathway and kinetics of crystallization of the melt are strongly related to the kinetics of the LLT. Our work provides new insights into the vitrification process and the kinetics of crystallization, and contributes to designing more stable metallic glasses.

© 2020 Acta Materialia Inc. Published by Elsevier Ltd. All rights reserved.

The unsatisfactory glass-forming ability is a major bottleneck of the structural application of metallic glasses even though they show superior mechanical properties [1,2]. Over the past half century, profound studies bring a series of breakthroughs in GFA of metallic glass, which also deepen the fundamental understanding of the glass formation and crystallization process [3–5]. As the formation of glass is a competing process between supercooled liquid and crystalline phases, the understanding of GFA is mainly examined through the lens of classical nucleation theory (CNT), where GFA is related to the crystal nucleation rate per unit volume,  $I_n$ , and low nucleation rate means good GFA [6–10]. Here  $I_n$  is expressed as  $I_n = \frac{A_v}{\eta(T)} \exp\left(-\frac{16\pi\sigma^3}{3k_B T |\Delta g(T)|^2}\right)$ , where  $A_v$  is a constant,  $\eta(T)$  is the viscosity of undercooled liquid,  $\sigma$  is the interfacial energy between liquid and nuclei and  $\Delta g(T)$  is the free energy difference between liquid and crystalline phases. Therefore, the evolution of the supercooled liquid and the differences between the supercooled liquid and crystalline phases are commonly believed

to be the most important factors affecting GFA [7,11]. However, growing evidences of multistep nucleation with much higher nucleation rate contradict the basic assumption of CNT, suggesting that the CNT encounters some limitations in the interpretation of the kinetics and pathway of crystallization [12–16]. These limitations strongly indicate that the current understandings of GFA are far from comprehensive. Recently, more factors have been taken into consideration [17–20], while there are still many issues about GFA which are not well understood.

Among all the factors that may affect GFA, the evolution of the alloy melt above its liquidus temperature  $T_{liq}$  is the least considered. The main reason is that the equilibrium melt is commonly thought as a simple liquid with a very short ( $\sim 10^{-13}$  s) relaxation time. It seems impossible that the changes in the melt above  $T_{liq}$  could affect the behaviors of undercooled liquid, let alone the crystallization process [21]. Thus, it is commonly accepted that the GFA is irrelevant to the state of equilibrium melt.

However, the situation could be quite different for the alloy melt with a liquid-liquid transition taking place above  $T_{liq}$ . Contrary to the conventional understanding, this melt is very complex, and exhibits two distinct liquid phases [22]. In addition, the transition between the two liquids shows the characteristics of first-

E-mail addresses: [ensiyu@mail.hust.edu.cn](mailto:ensiyu@mail.hust.edu.cn) (Y. Yu), [liu2000@mail.hust.edu.cn](mailto:liu2000@mail.hust.edu.cn) (L. Liu).

\* Corresponding authors.

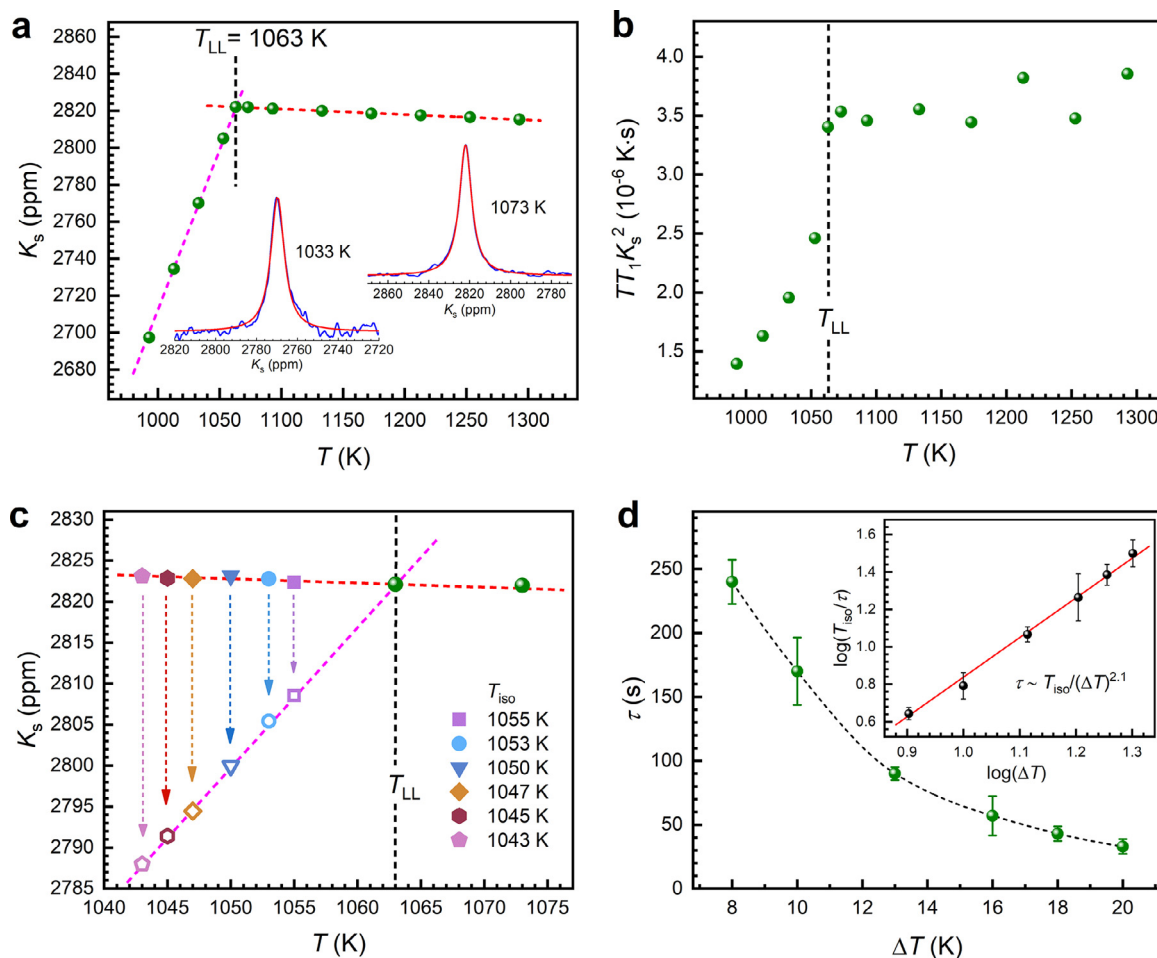


**Fig. 1.** Liquid-liquid transition in the equilibrium  $\text{Pd}_{42.5}\text{Ni}_{42.5}\text{P}_{15}$  melt characterized by NMR. (a) Temperature dependence of  $^{31}\text{P}$  Knight shift ( $K_s$ ). The two linear fits (red and pink dashed lines) intersect at 1063 K. The insets are two typical spectra (blue line) above and below the transition temperature with the Lorentzian fitting of the spectrum (red line). (b) Value of  $TT_1K_s^2$  as a function of temperature. (c) The changes of  $K_s$  at different undercooled temperatures  $T_{iso}$  after quenching the melt from 1173 K. The solid and open symbols represent the initial and equilibrium  $K_s$ , respectively. (d) The average incubation time  $\tau$  versus degree of undercooling  $\Delta T = 1063 - T_{iso}$ . The inset plots  $\log(T_{iso}/\tau)$  versus  $\log(\Delta T)$  and the slope of the linear fit is 2.1. (For interpretation of the references to color in this figure legend, the reader is referred to the web version of this article.)

order phase transition, which implies that both liquid states could be undercooled to the temperature far below  $T_{liq}$ , even approaching the glass transition temperature  $T_g$ . Consequently, the influences of the complexity of the alloy melts together with the kinetics of the first-order LLT on the GFA should be taken into consideration.

Herein, a glass-forming alloy of  $\text{Pd}_{42.5}\text{Ni}_{42.5}\text{P}_{15}$  is selected, and the influence of LLT on its GFA is studied. The liquidus temperature of the  $\text{Pd}_{42.5}\text{Ni}_{42.5}\text{P}_{15}$  system was determined as 993 K by the flash differential scanning calorimetry (FDSC) (Fig. S1). In situ  $^{31}\text{P}$  high-temperature nuclear magnetic resonance (NMR) was carried out to characterize the LLT above  $T_{liq}$ . Firstly, step cooling experiments were conducted, in which the  $\text{Pd}_{42.5}\text{Ni}_{42.5}\text{P}_{15}$  alloy was first heated to 1293 K and held there for 30 min for homogenization, and then it was cooled step by step to 993 K with 40 K interval in the range of 1293 ~ 1093 K and 20 K interval below 1053 K. NMR spectra were taken isothermally after equilibrating for 30 min at each step. The peak position of each spectrum, the Knight shift ( $K_s$ ), which is determined by the ensemble average of local magnetic field around  $^{31}\text{P}$  nuclei and sensitive to the changes in structure [22,23], is plotted in Fig. 1a as a function of temperature ( $T$ ).  $K_s$  varies linearly above 1063 K with a slope of -0.03 ppm/K (red line), but with a slope of 1.73 ppm/K (pink line) below 1063 K, indicating a significant change in the P-centered local structures.

This result implies that an LLT may take place at  $T_{LL} = 1063$  K. Two typical  $^{31}\text{P}$  spectra above and below  $T_{LL}$  are shown in the insets of Fig. 1a. Each spectrum is a single Lorentzian peak and the integral areas of the peaks remain identical, indicating that the system above or below  $T_{LL}$  is a homogeneous liquid without any loss of the contributing P atoms.

In an ideal metallic liquid, the magnetic coupling between nuclei and s-like conduction electrons through the Fermi contact interaction is the dominant mechanism of both Knight shift and spin-lattice relaxation, leading to the Korringa relation  $TT_1K_s^2 = \frac{\hbar\gamma_e^2}{4\pi k_B\gamma_n^2} f$ , where  $T_1$  is the spin-lattice relaxation time (Fig. S2),  $\gamma_e$  and  $\gamma_n$  are respectively the electron and nucleus gyromagnetic ratio,  $\hbar$  and  $k_B$  are respectively the reduced Planck and Boltzmann constant, and  $f$  is a constant related to the electron-electron interaction [24–26]. Thus, the value of  $TT_1K_s^2$  is supposed to be a constant. However, in the presence of strong covalent bonds, the electrons tend to be localized, remaining in the vicinity of nuclei for longer time, and thus the spin-lattice relaxation process would be more efficient. Therefore, the actual relaxation time  $T_1$  is shorter compared with the case in ideal metallic liquid, leading to the breakdown of Korringa relation [27,28]. Fig. 1b plots the value of  $TT_1K_s^2$  versus  $T$ , which is almost constant above 1063 K, but drops substantially below 1063 K with decreasing temperature, indicating the breakdown of Korringa relation. This result suggests

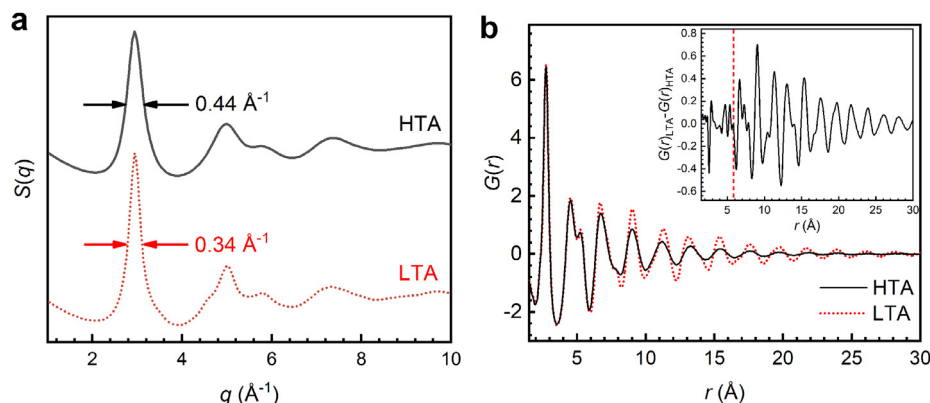


**Fig. 2.** Structural difference of HTA and LTA characterized by high-energy synchrotron XRD. (a) Structure factors  $S(q)$  of HTA and LTA. (b) Pair correlation functions  $G(r)$  of HTA and LTA. The inset shows the difference in  $G(r)$  between LTA and HTA.

that the covalent bonding in the liquid is significantly enhanced below 1063 K, which could be the structural origination of the LLT.

Further, the kinetics associated with the LLT was examined. The sample was heated to 1173 K and held there isothermally for 30 min, and then fast cooled to one of the undercooled temperature (with respect to  $T_{LL} = 1063$  K)  $T_{iso} = 1055, 1053, 1050, 1047, 1045$ , and  $1043$  K in about 1.5 min, and held there isothermally. Once the temperature stabilized at each  $T_{iso}$ , NMR spectra were recorded every 10 s to monitor any possible transition. Fig. 1c shows the measured  $K_s$  at different  $T_{iso}$ . When reaching  $T_{iso}$ ,  $K_s$  initially follows the linear extrapolation (red line) of the  $T$ -dependent  $K_s$  above 1063 K measured in the step cooling experiments. After a certain incubation time  $\tau$ ,  $K_s$  starts to jump to the expected value determined by the linear fit of the  $T$ -dependent  $K_s$  below 1063 K (pink line). These results clearly show that the stable liquid above 1063 K (high-temperature liquid, named as HTL) can be undercooled below  $T_{LL}$  and finally transforms to the stable liquid below 1063 K (low-temperature liquid, named as LTL). Such behavior is consistent with the first-order phase transition [29]. The average incubation time  $\tau$  of three independent measurements at each temperature versus the degree of undercooling  $\Delta T = T_{LL} - T_{iso}$  is shown in Fig. 1d. As  $\Delta T$  increases from 8 to 20 K (i.e.,  $T_{iso}$  decreases from 1055 to 1043 K), the incubation time decreases rapidly from 240 s to 30 s. The inset shows the plot of  $\log(T_{iso} / \tau)$  versus  $\log(\Delta T)$ , which can be well fitted with a linear function, indicating a power-law relation of  $\tau \propto T_{iso}/(\Delta T)^m$  with  $m = 2.1$ . Similar power-law was also observed in the LLTs in  $\text{La}_{50}\text{Al}_{35}\text{Ni}_{15}$  liquid [22] and molten sodium acetate trihydrate [30].

To further explore the difference between HTL and LTL, two glassy samples, labeled as HTA and LTA accordingly, were prepared by quenching the melt from 1223 K (above  $T_{LL}$ ) and 1023 K (below  $T_{LL}$ ) using melt-spinning technique, respectively. High-energy synchrotron X-ray diffraction (XRD) was then employed to examine the structure of the two glassy samples. As shown in Fig. 2a, no sharp Bragg peaks corresponding to any crystallites are detected on the structure factors  $S(q)$ , confirming the amorphous nature of the two samples. These results are consistent with the high-resolution transmission electron microscopy (HRTEM) results (Fig. S3). The full width at half maximum (FWHM) of the first peak in  $S(q)$  are about  $0.44 \text{ \AA}^{-1}$  and  $0.34 \text{ \AA}^{-1}$  for HTA and LTA, respectively. The narrower FWHM of LTA suggests the existence of more ordered structures in this glass. The structural details can be better appreciated from real space analysis by looking at the pair correlation function  $G(r)$  obtained by the Fourier transformation of the corresponding  $S(q)$  (Fig. 2b). The positions difference of the first

maxima of  $G(r)$  is very subtle ( $2.75 \text{ \AA}$  for LTA and  $2.74 \text{ \AA}$  for HTA). The increased order in the structure of the LTA is reflected in well-defined oscillations up to the 12<sup>th</sup> shell in the LTA while only up to the 8<sup>th</sup> shell in the HTA. This behavior is clearly identified from the difference in  $G(r)$  between HTA and LTA, obtained by subtracting the former from the latter (inset of Fig. 2b). The difference between these two  $G(r)$  curves are negligible up to the second minimum distance ( $r < 5.9 \text{ \AA}$ ), but beyond this distance, LTA shows an enhanced correlation which is still pronounced even up to  $r > 25 \text{ \AA}$ . These results suggest that the structure of short-range clusters in LTA and HTA are almost the same, but a more pronounced medium-range ordering presents in LTA.

LLTs were supposed to take place in several metallic glass-forming liquids, but the structural mechanism associated with the LLT was not clear [31–33]. NMR observables are sensitive to the interaction between electrons and nuclei, and can provide information of all nearest-neighbor atoms surrounding the atom and possibly beyond. Combined with the evidence of synchrotron XRD, more detailed structural changes can be revealed. Since the glass is commonly considered as “frozen liquid”, the results of HTA and LTA imply that the structures of short-range clusters in LTL and HTL could be almost identical, but the correlation between the short-range clusters in LTL and HTL should be different. Recalling the significantly enhanced covalent bonding in LTL suggested by the breakdown of Korringa relation (Fig. 1b), it is reasonable to assume that the transition from HTL to LTL is associated with the increase of the short-range clusters and stronger correlation between the clusters, consistent with the two-order-parameter model [34,35].

The GFA of the two liquids were examined by FDSC experiments through measuring the critical cooling rate  $R_c$ , which is the slowest cooling rate at which equilibrium liquid can be quenched into glass without detectable crystallites, and a lower  $R_c$  stands for a better GFA [36,37]. The sample was first heated to a predetermined temperature  $T_q = 1073$  K (i.e., 10 K above  $T_{LL}$ ) at a constant rate of 100 K/s and kept there isothermally for 30 s, then cooled to room temperature at a series of cooling rate  $q^-$  (50 ~ 40000 K/s) to obtain samples with different content of amorphous phase. After this pretreatment, the contents of amorphous phase in these samples were measured by FDSC via heating each sample from room temperature to 1073 K at a constant rate of 100 K/s (see the inset of Fig. 3a for temperature protocol). For comparison, these procedures were repeated for  $T_q = 1023$  K (i.e., 40 K below  $T_{LL}$ ). Fig. 3a shows a representative DSC heating curve for the sample obtained from  $T_q = 1073$  K and  $q^- = 40000$  K/s. The two exothermic peaks (around 685 K and 770 K) are related to the polyamorphic transition [38,39] and the crystallization of the amorphous phase, re-

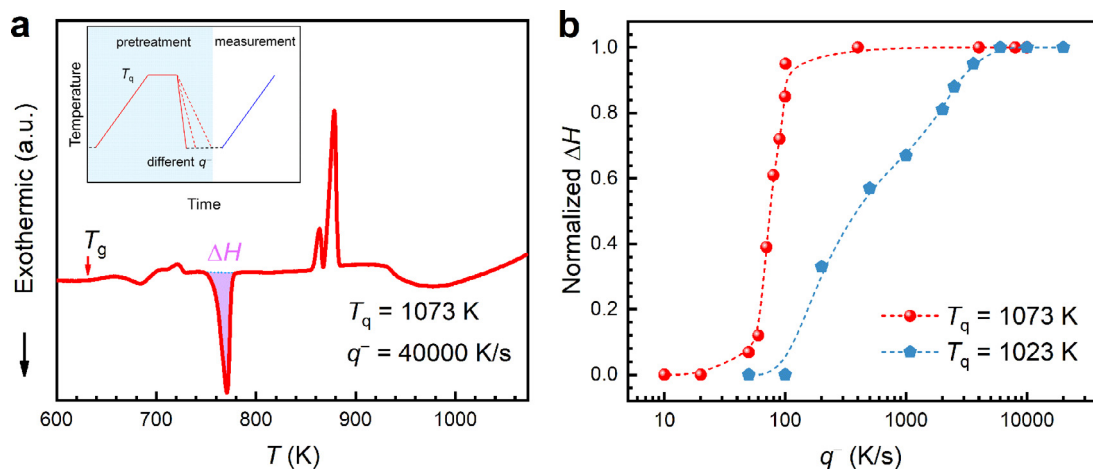


**Fig. 3.** Glass-forming ability of the two liquids characterized by FDSC. (a) A typical FDSC heating curve of the sample obtained from  $T_q = 1073$  K and  $q^- = 40000$  K. The enthalpy of crystallization is denoted as  $\Delta H$ . The inset shows the temperature protocol of the FDSC experiments. (b) The content of amorphous phase as a function of cooling rate  $q^-$  of the samples obtained from  $T_q = 1073$  K and 1023 K, respectively.

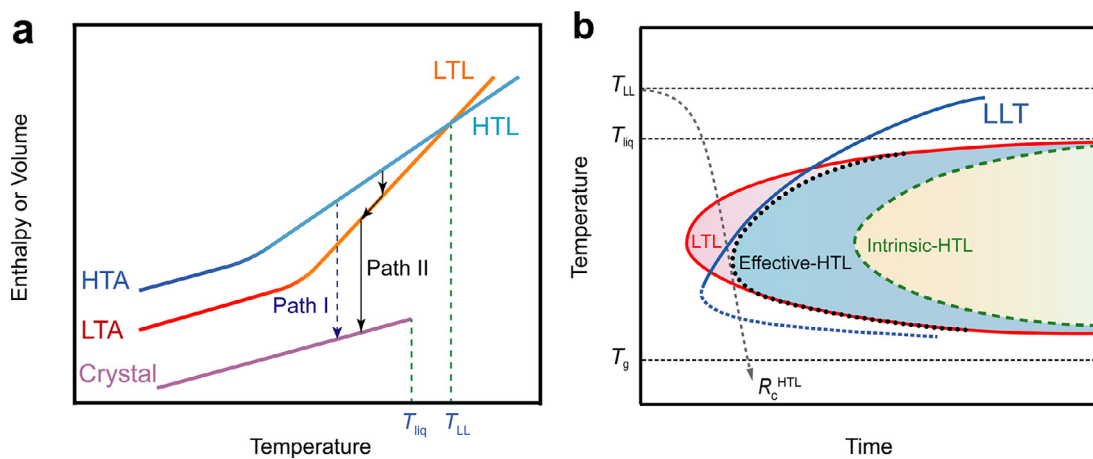


**Fig. 4.** Effects of LLT on the pathways and kinetics of crystallization. (a) Schematic evolution of enthalpy or volume upon cooling the melt. (b) Mechanism of the different GFA of HTL and LTL. The red and green dashed lines represent the intrinsic crystallization TTT curve of LTL and HTL, respectively. The cerulean line represents the TTT curve of LLT. The TTT curve of LLT intersects the TTT curve of LTL at high and low temperature and the black dotted line denotes the effective crystallization TTT curve of HTL.  $R_c^{\text{HTL}}$  is the critical cooling rate to bypass the effective TTT curve of HTL. (For interpretation of the references to color in this figure legend, the reader is referred to the web version of this article.)

spectively, and the endothermic peaks (around 880 K) represent the melting process. Fig. 3b plots the area of the second exothermic peak ( $\Delta H$ ) versus  $T$ . Here,  $\Delta H$  of each sample was normalized to that of the sample obtained from  $T_q = 1073$  K and  $q^- = 40000$  K/s (this sample was used as the reference because it is fully amorphous, see the discussion below), and this value is directly proportional to the content of amorphous phase in each sample. For samples cooled from  $T_q = 1023$  K (i.e., from LTL), the content of amorphous phase does not change when  $q^- > 6000$  K/s, but drops significantly when  $q^- < 6000$  K/s, suggesting that  $R_c$  is about 6000 K/s for LTL. However, for samples cooled from  $T_q = 1073$  K (i.e., from HTL), the content of amorphous phase remains constant until  $q^- < 100$  K/s, indicating that  $R_c$  is about 100 K/s for HTL. The results demonstrate clearly that HTL exhibits much better GFA compared to LTL.

The significance of the current experiments is that the GFA is observed to be closely related to the liquid-liquid transition event. It is shown unambiguously that an alloy melt can exhibit two significantly different GFA without change in composition. Due to the first-order nature of the LLT, both HTL and LTL can be maintained to the temperature far below  $T_{\text{liq}}$ , and further vitrified into differ-

ent glasses (Fig. 2a). The evolutions of the two liquids are schematically shown in Fig. 4a. As HTL and LTL are distinct liquid states, it is reasonable that they show different crystallization kinetics and hence different GFAs.

The LLT plays a crucial role in the crystallization of HTL. On the one hand, it provides an alternative crystallization pathway for HTL. The crystallization of HTL would follow one of the two possible pathways: either crystallize directly from HTL state (Path I in Fig. 4a), or crystallize via LTL after the LLT takes place (Path II in Fig. 4a). In the latter case, the supercooled LTL acts as an intermediate state between the supercooled HTL and crystalline state. The existence of Path II is coincident with previous studies [38,39], where it was suggested that the HTA transformed firstly to a supercooled liquid (supercooled liquid I) above its glass transition temperature, and then to another supercooled liquid (supercooled liquid II) before crystallization upon further heating. Although the supercooled liquid I and II are not cognized in detail, they are consistent with the supercooled HTL and LTL in our picture shown in Fig. 4a, respectively. Thus, our experiments suggest a new possible crystallization pathway upon cooling, i.e., crystallize via an intermediate liquid state (Path II).



On the other hand, the LLT may also change the crystallization kinetics of HTL. The selection of the crystallization pathway is determined by the competition between the kinetics of LLT and the crystallization kinetics of HTL. Once the incubation time of LLT is shorter than that of the crystallization of HTL, HTL would crystallize through Path II. Fig. 4b schematically shows a possible relationship between the crystallization time-temperature-transformation (TTT) curves of HTL (green dashed line) and LTL (red line), together with the TTT curve of LLT (cerulean line). Here, the critical cooling rate of HTL,  $R_c^{\text{HTL}}$ , is no longer related to the intrinsic TTT curve of HTL, but related to the effective-TTT curve (dark dotted line), which is the superposition of the TTT curve of LLT and the crystallization TTT curve of LTL, with its nose point around the lower intersection of the two curves. The minimum cooling rate to bypass this effective-TTT curve can be determined as  $R_c = (T_{\text{LL}} - T_{\text{en}}^{\text{HTL}})/t_{\text{en}}^{\text{HTL}}$ , where  $T_{\text{en}}^{\text{HTL}}$  and  $t_{\text{en}}^{\text{HTL}}$  are the temperature and time scale at the nose point. By assuming that  $T_{\text{en}}^{\text{HTL}}$  is around the nose temperature  $T_n^{\text{LTL}}$  of the TTT curve of LTL, which can be estimated as  $T_n^{\text{LTL}} = T_g + 0.5(T_{\text{liq}} - T_g) = 780 \text{ K}$  [40] and  $t_{\text{en}}^{\text{HTL}}$  deduced from the continuous-cooling-transformation (CCT) curve of LLT constructed by the method developed by Grange and Keifer [41], is about 1.4 s (Fig. S4),  $R_c$  can be roughly estimated as 200 K/s. To our great surprise, this value is very close to the  $R_c^{\text{HTL}}$  acquired from the FDSC experiments. This result strongly indicates that the picture described in Fig. 4b could be the case of the crystallization in  $\text{Pd}_{42.5}\text{Ni}_{42.5}\text{P}_{15}$ .

It is of interest to note that HTL exhibits a better GFA than LTL. Although the detailed kinetics of the direct crystallization process of HTL is experimentally unachievable due to the interference of LLT, it can be concluded qualitatively from the poor GFA of LTL that the crystal nucleation rate per unit volume  $I_n$  from LTL should be much higher than that from HTL. This may result from the formation of the clusters with medium-range ordering in the supercooled LTL, and such clusters may act as precursors for the nucleation of the crystalline phase [11], reducing the interfacial energy  $\sigma$  and leading to a lower energy barrier for the formation of the crystal nuclei and hence the poor GFA of LTL.

In summary, our in situ high-temperature NMR studies show that the glass-forming liquid  $\text{Pd}_{42.5}\text{Ni}_{42.5}\text{P}_{15}$  presents a first-order LLT at the temperature of 1063 K, high above the liquidus temperature of 993 K, accompanied by a drastic enhancement of the covalent bonding below 1063 K. The two liquids can be vitrified into two corresponding glasses which are different in the medium-range ordering rather than the structure of short-range clusters. These results suggest that the LLT may be a result of the increase of the short-range clusters. The FDSC studies reveal that the high-temperature liquid exhibits much better GFA than the low-temperature liquid, which may be ascribed to the enhancement of medium-range ordering in the supercooled LTL. Further analyses indicate that the LLT can provide an indirect crystallization pathway for HTL, and moreover, the kinetics of LLT has a significant influence on the GFA. This effects of LLT provides a new way for future study of the process of crystallization and is also important for the fabrication of metallic glasses. What is more, our work may also provide an alternative understanding for some traditional phenomena. For instance, many metallic glass-forming liquids exhibit overheating effects, where the nucleation behavior of the system or the mechanical properties of the metallic glasses show markedly difference with different overheating temperature [42,43]. Till now, there are only qualitative understandings for these phenomena. It is proposed to be related to the heterogeneities in the liquid, which dissolve above a threshold temperature. However, such behavior

could be quantitatively explained within our LLT scenario, where  $T_{\text{LL}}$  is the threshold temperature.

## Declaration of Competing Interest

The authors declare that they have no known competing financial interests or personal relationships that could have appeared to influence the work reported in this paper.

## Acknowledgement

The authors are grateful to the Analytical and Testing Center of HUST for technical assistance. This work was financially supported by the National Natural Science Foundation of China (grant no. 51872105).

## Supplementary materials

Supplementary material associated with this article can be found, in the online version, at doi:10.1016/j.scriptamat.2020.10.042.

## References

- [1] W.H. Wang, C. Dong, C.H. Shek, Mater. Sci. Eng. R. Rep. 44 (2) (2004) 45–89.
- [2] M. Telford, Mater. Today 7 (3) (2004) 36–43.
- [3] A.L. Greer, Science 267 (5206) (1995) 1947.
- [4] Y. Li, Q. Guo, J.A. Kalb, C.V. Thompson, Science 322 (5909) (2008) 1816.
- [5] C.G. Tang, P. Harrowell, Nat. Mater. 12 (6) (2013) 507–511.
- [6] M.H. Cohen, D. Turnbull, J. Chem. Phys. 31 (5) (1959) 1164–1169.
- [7] D. Turnbull, Contemp. Phys. 10 (5) (1969) 473–488.
- [8] A. Inoue, Acta Mater. 48 (1) (2000) 279–306.
- [9] Z.P. Lu, C.T. Liu, Acta Mater. 50 (13) (2002) 3501–3512.
- [10] D.M. Herlach, Mater. Sci. Eng. R. Rep. 12 (4) (1994) 177–272.
- [11] J. Russo, F. Romano, H. Tanaka, Phys. Rev. X 8 (2) (2018) 021040.
- [12] D. Erdemir, A.Y. Lee, A.S. Myerson, Acc. Chem. Res. 42 (5) (2009) 621–629.
- [13] P.G. Vekilov, Cryst. Growth Des. 10 (12) (2010) 5007–5019.
- [14] J. De Yoreo, Nat. Mater. 12 (4) (2013) 284–285.
- [15] J. Lee, J. Yang, S.G. Kwon, T. Hyeon, Nat. Rev. Mater. 1 (8) (2016) 16034.
- [16] J.J. De Yoreo, P.U.P.A. Gilbert, N.A.J.M. Sommerdijk, et al., Science 349 (6247) (2015) aaa6760.
- [17] P. Zalden, F. Quirin, M. Schumacher, et al., Science 364 (6445) (2019) 1062.
- [18] S. Wei, G.J. Coleman, P. Lucas, C.A. Angell, Phys. Rev. Appl. 7 (3) (2017) 034035.
- [19] J. Schroers, W.L. Johnson, J. Appl. Phys. 88 (1) (2000) 44–48.
- [20] J. Schroers, Y. Wu, R. Busch, W.L. Johnson, Acta Mater. 49 (14) (2001) 2773–2781.
- [21] A. Cavagna, Phys. Rep. 476 (4) (2009) 51–124.
- [22] W. Xu, M.T. Sandor, Y. Yu, et al., Nat. Commun. 6 (2015) 7696.
- [23] L.L. Li, J. Schroers, Y. Wu, Phys. Rev. Lett. 91 (26) (2003) 265502.
- [24] A. Abragam, Principles of Nuclear Magnetism, Clarendon Press, Oxford, 1961.
- [25] C.P. Slichter, Principles of Magnetic Resonance, Harper & Row Publishers, New York, 1963.
- [26] J. Korringa, Physica 16 (7) (1950) 601–610.
- [27] W.W. Warren, Phys. Rev. B 3 (11) (1971) 3708–3724.
- [28] R. Dupree, D.J. Kirby, W. Freyland, Philos. Mag. B 46 (6) (1982) 595–606.
- [29] D. Turnbull, in: Solid State Physics, Elsevier, 1956, pp. 225–306.
- [30] X. Liu, S.Y. Liu, E.Y. Chen, et al., J. Phys. Chem. Lett. 10 (15) (2019) 4285–4290.
- [31] C. Way, P. Wadhwa, R. Busch, Acta Mater. 55 (9) (2007) 2977–2983.
- [32] S. Wei, F. Yang, J. Bednarcik, et al., Nat. Commun. 4 (2013) 2083.
- [33] M.E. Blodgett, T. Egami, Z. Nussinov, K.F. Kelton, Sci. Rep. 5 (1) (2015) 13837.
- [34] H. Tanaka, Phys. Rev. E 62 (5) (2000) 6968–6976.
- [35] H. Tanaka, Eur. Phys. J. E 35 (10) (2012) 113.
- [36] C.S. Ray, S.T. Reis, R.K. Brow, et al., J. Non-Cryst. Solids 351 (16) (2005) 1350–1358.
- [37] Q.J. Zheng, Y.F. Zhang, M. Montazerian, et al., Chem. Rev. 119 (13) (2019) 7848–7939.
- [38] S. Lan, Y. Ren, X.Y. Wei, et al., Nat. Commun. 8 (2017) 14679.
- [39] Q. Du, X.J. Liu, H.Y. Fan, et al., Mater. Today 34 (2020) 66–77.
- [40] Z.P. Lu, C.T. Liu, Phys. Rev. Lett. 91 (11) (2003) 115505.
- [41] R. Grange, J. Kiefer, Trans. ASM 29 (1) (1941) 85.
- [42] S. Mukherjee, Z. Zhou, J. Schroers, et al., Appl. Phys. Lett. 84 (24) (2004) 5010–5012.
- [43] Y. Zhao, S. Kou, H. Suo, et al., Mater. Des. 31 (2) (2010) 1029–1032.